60 GHz Temporal Dispersion Characteristics with Different Antenna Polarizations in an Underground Mine

Shah Ahsanuzzaman Md Tariq*, Charles L. Despins†, Sofiène Affes‡,Chahé Nerguizian*
*Université de Montréal-École Polytechnique, Montreal, Canada
†Université du Québec-École de Technologie Supérieure, Montreal, Canada
‡Université du Québec-Institut National de la Recherche Scientifique, Montreal, Canada
Emails: {tariq.shah-ahsanuzzaman-md, chahe.nerguizian}@polymtl.ca

***Abstract*—This paper presents the measurements results of a 60 GHz wireless channel in underground mine galleries at depths of 40 m and 70 m. Different antenna polarizations and configurations were considered in this study. Results show that the rough surface scattering and the gallery dimensions of the underground mine significantly impact on the time dispersion characteristics. Particularly, a vertical antenna configuration provides a larger number of multipath than a horizontal one. Due to the fact of gallery dimension and surface roughness characteristics, the 70 m-depth gallery provides a lower value of delay spread and more time variation phenomenon than the 40 m-depth. Omnidirectional antenna configurations are also shown to be not feasible for point to point link. The characteristics of the power delay profile of the scattered channel based on the antenna radiation pattern and impact on its time dispersion are discussed.**

***Index Terms*—60 GHz channel measurements, underground mine, antenna polarization, time dispersion.**

I. Introduction

Short distance wireless communication research at 60 GHz is recently taken into account for future indoor high-speed communication. 60 GHz frequency provides a short range, a low interference, and a beamforming capability due to its available higher attenuation phenomenon, higher bandwidth and achievable narrow beamwidth. These features could offer Gigabit per second speed for short range point to point and long range backhaul link. However, the application of this frequency can also be injected into a confined environment such as underground mine. For instance, a high speed backhaul link through the entire gallery could be useful to deploy a wireless network. Moreover, some service-centric applications with its higher bandwidth such as high precision in geolocalization of miners and equipment, low latency real-time video communication are particularly the growing needs of the mining industry.

Work supported by an NSERC/Bell Alliant/Newtrax CRD Project on smart Mines and NSERC CREATE PERSWADE Research Training Program. Most recent results of this work, disclosed herein and in the PhD thesis of the first author [1], have never been published nor presented previously in any conference vanue.

The CANMET mine, operated by LRTCS laboratory, located in Val-d'Or, has been used for measurements to design and improve mining industry wireless communications systems in different frequencies. Nerguizian et al. [2] found around 27 ns Root Mean Square (RMS) delay spread at 2.4 GHz and Boutin et al. [3] compared measurement results between 2.4 GHz and 5.8 GHz and reported that the higher frequency bands tend to provide lower RMS delay spread values. Moreover, no correlation of RMS delay spread with respect to transmitter (Tx) and receiver (Rx) antenna separation distances, as well as no clustering effect of impulse responses were observed. As well, measurements at 60 GHz in the CANMET mine were previously performed by the LRTCS laboratory reported in [4], [5]. Till now, measurements with different antenna polarizations and different antenna configurations at 60 GHz in both measurable galleries have not been addressed.

On the other hand, measurements at 60 GHz in the residential environments show that circular polarization may provide better bit error rate (BER) performance than linear polarization [6]. Measurement results also show that the horizontal (H) and vertical (V) polarization types depend on the number of strong reflected waves [7]. Manabe [8] found that the RMS delay spread value with horizontal polarization is slightly lower than with vertical polarization. The IEEE 802.15.3c Task Group also demonstrated that the polarization mismatch may degrade the received power by 10 to 20 dB [9]. Co and Cross polarization discrimination are studied with an intention to use polarization diversity and dual polarization to achieve a high capacity wireless communication system in a hazard environment.

Measurement results in underground mine and tunnels at lower frequencies with antenna polarizations show that different polarizations provide different coupling losses, attenuations and bend losses [10], [11]. With 5 mm wavelength the scattering phenomenon may occur in a confined environment. To deploy a wireless system, the channel characteristics with antenna polarizations

(a)

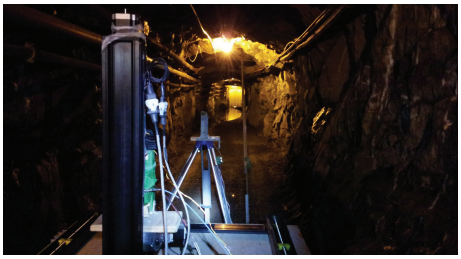

(b)

Fig. 1. (a) and (b) are the 40 m and 70 m mine gallery, respectively.

are necessary to be addressed in the channel model, particularly where the surface roughness and gallery passages are different within a short area. Measurements with antenna polarizations are motivated by the Co (Tx-V, Rx-V or Tx-H, Rx-H) polarization antenna radiation patterns and the different magnitude of the floor, wall and ceiling roughness.

II. Measurement Campaign, Setup and Data Post Processing

In the campaign area of the CANMET mine as shown in Fig. 1, the height and width and length of the 40 m depth gallery were around 5 m, 5 m, 30 m, whereas 2.5 m, 3 m, 70 m were at 70 m depth gallery, respectively. In order to find channel frequency response $H(f)$, a 60 GHz frequency domain wideband measurement system setup with a Vector Network Analyzer (VNA-ANRITSU MS 4647A) was used. The center frequency and bandwidth were 58.32 GHz and 2.16 GHz, respectively. The SOLT (short-open-load-thru) calibration was done with 2000 frequency sweep points with a sampling frequency of 1.08 MHz. In both galleries, the Tx and Rx heights were 1.5 m. Hence, the distances between antennas and walls, ceiling, and floor of the 40 m depth gallery were around 2.5 m, 3.5 m, 1.5 m, whereas 1.5 m, 1 m, 1.5 m were at 70 m depth gallery, respectively. The Tx was fixed and the Rx was moved every 20 cm along the gallery length (32 points). At each 20 cm Tx - Rx seperation distance, three consequitive measurements seperated by $\lambda/2$ with 15 snapshots in different time instant were taken to avoide space and time varying fading, respectively. A camera tripod and a laser were used to have the accurate position of the point to point link. By connecting a computer to the VNA via a GPIB interface was used for data acquisition. The description of the campaign, the experimental setup and its parameters are described in [12]–[14]. For the data post-processing of each configuration, 96 (32×3) frequency responses were obtained at each position d by averaging 15 snapshots. The over the air (OTA) calibration was performed dividing 96 complex-valued frequency responses by OTA 1 m complex-valued frequency response. With 0.46 ns value of the time resolution τ and using the Inverse Fast Fourier Transform (IFFT), the normalized channel impulse responses $h(\tau, d)$ were obtained from the OTA calibrated frequency responses using the procedure employed in [3], [12], [13]. The Power Delay Profiles (PDPs) were calculated by $P(\tau, d) = |h(\tau, d)|^2$. The noise threshold level was set to -25 dB.

III. Time Dispersion Characteristics of the Scattered Channel

To analyze the time dispersion characteristics of the scattered channel, the time resolution (which is the inverse of the bandwidth) of 0.46 ns is taken to consider all scattered paths. The extracted number of multipath components (by calculating the number of peaks and inflections [3] from the impulse responses). The calculated RMS delay spread [15] with respect to Tx - Rx distance are illustrated in Fig. 2. Results show that the relationship between the number of multipath and the distance exhibits a random behavior and observed a little trend of decrement in the 40 m gallery in both polarization configurations. The number of paths remains random and observed a little trend of constant at 70 m. The number of multipath were found less valued at 70 m gallery than 40 m gallery. Moreover, the horizontal polarization of the Omnidirectional antenna configuration results exhibited less multipath compared to the vertical polarization. The RMS delay spread values were found to behave randomly according to Tx - Rx distance. Fig. 3 depicts the cumulative distribution plot of measured RMS delay spread and coherence bandwidth. $Bc_{0.9}$ (i.e., frequency shift where correlation level falls at 90%) has been extracted from the frequency correlation function of the measured PDPs as per the expressions are given in [16]. The mean (μ) and the standard deviation (σ) of the time dispersion results of the channel such as RMS delay spread (τ_{rms}), mean access delay ($\overline{\tau}$), maximum access delay (τ_{max}) and coherence bandwidth ($Bc_{0.9}$) are listed in Table I. Results suggest that a wider gallery dimension provides a higher RMS delay spread than a narrower gallery. In both galleries, the VV polarization also provides a higher RMS delay spread than the HH polarization. The mean value of $Bc_{0.9}$ remains around 30 at 40 m gallery for VV polarization. In the 70 m gallery, the $Bc_{0.9}$ fluctuates a little and the average value remains around 90 MHz with VV polarization. This difference occurred due to the wider gallery dimension at 40 m compared to the 70 m level. The higher values

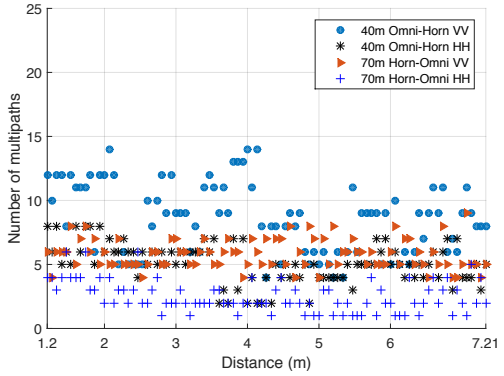

(a)

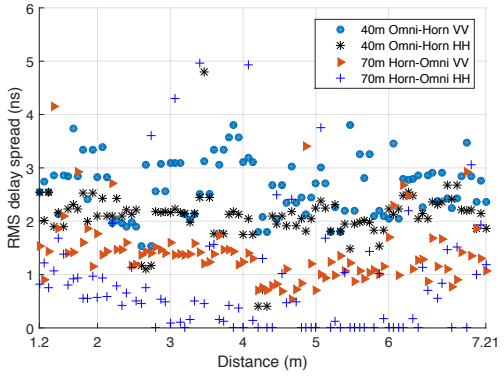

(b)

Fig. 2. Scatter plot of time dispersion characteristics with different antenna and polarization configurations. (a) the number of multipath, (b) the RMS delay spread, with respect to Tx - Rx distance.

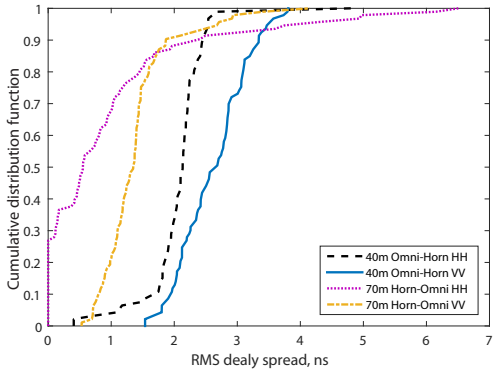

(a)

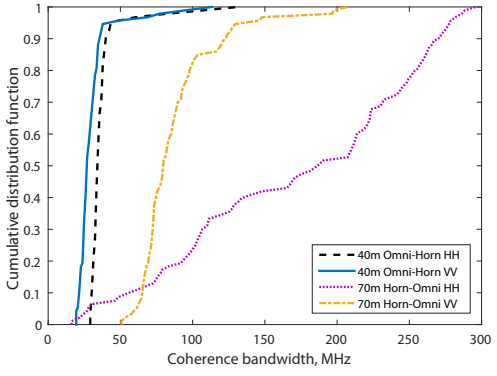

(b)

Fig. 3. CDF of RMS delay spread and coherence bandwidth (i.e. $Bc_{0.9}$) in both galleries. (a) the RMS delay spread, (b) the coherence bandwidth.

TABLE I
TIME DISPERSION RESULTS.

Configuration	τ_{rms} (ns)		$\overline{\tau}$ (ns)		τ_{max} (ns)		Bc_{90} (MHz)	
	μ	σ	μ	σ	μ	σ	μ	σ
40 $m_{O-H_{HH}}$	2.04	0.40	1.52	0.53	6.51	1.89	37.78	15.46
40 $m_{O-H_{VV}}$	2.63	0.53	2.05	0.69	11.34	3.47	30.85	14.83
70 $m_{H-O_{HH}}$	0.97	1.33	0.21	0.25	7.32	11.31	172.75	81.14
70 $m_{H-O_{VV}}$	1.39	0.58	0.59	0.29	9.88	7.47	88.18	28.45

Note: $H/O - H/O_{HH/VV}$ denotes Horn / Omni - Horn / Omni with horizontal - horizontal / vertical - vertical configuration.

of standard deviations of the time dispersion results suggest that 70 m gallery is more time dispersive than 40 m gallery due to its narrower gallery dimension with roughness (e.g., which causes more scattering).

A. Comparison with other experimental work

Experimental results in CANMET underground mine with different system setups and configurations are listed in Table II. Ben Mabrouk et al. [4] reported an average of 7.65 ns RMS delay spread value in the 40 m gallery at 60 GHz, where 50° Half Power Beamwidth (HPBW) rectangular patch (2x2) antennas with 10 dBi gain in both Tx and Rx sides of a 2x2 MIMO system were used. In this paper, a lower value of RMS delay spread of 2.63 ns has been found in the same gallery when a SISO configuration has been employed with a 12° HPBW Rx pyramidal Horn antenna (24 dBi gain) and a Tx Omnidirectional antenna (3 dBi). The lower antenna gain provides a wider HPBW [17], resulting in the probability of having a higher number of multipath. Similarly, the experimental setup that has been used in [5] with Horn antennas and the results are listed in Table II. There is provided a different value of RMS delay spread from that of our work due to the difference of HPBW. In the considered measurement scenarios; surface wall, floor, and ceiling have different values of roughness and different gallery dimensions, and the use of different antenna polarizations, and the pointing ditections of both Tx and Rx antennas therefore could provide an impact on the time dispersion characteristics of the channel. This impact can be characterized by the different value of τ_{rms}.

IV. Effect of Time Dispersion Based on Antenna Radiation Patterns and Polarizations

To analyze the impact of the antenna polarizations on the scattered channel, the analytical explanations have

TABLE II
COMPARISON OF CANMET UNDERGROUND MINE EXPERIMENTAL RESULTS.

Reference	Mine gallery	Frequency (GHz)	Antenna system	Polarization	BW (GHz)	A_{tx}	A_{rx}	H_{tx}	H_{rx}	$\overline{\tau_{rms}}$ (ns)
[4]	40 m	60	MIMO	Vertical	7	Patch (2x2)	Patch (2x2)	50°	50°	7.65
[5]	70 m	2.46	SISO	Vertical	0.2	Omni	Omni	360°	360°	6.31
		5.8	SISO	Vertical	0.2	Omni	Omni	360°	360°	6.14
		60	SISO	Vertical	2	Horn	Horn	16°	16°	2.14
In this paper	40 m	60	SISO	Vertical	2.16	Omni	Horn	360°	12°	2.63
		60	SISO	Horizontal	2.16	Omni	Horn	$\simeq$ 40°	12°	2.044
	70 m	60	SISO	Vertical	2.16	Horn	Omni	12°	360°	1.39
		60	SISO	Horizontal	2.16	Horn	Omni	12°	$\simeq$ 40°	0.97

Note: In [4] a 2×2 MIMO antenna system configuration was used. In [5] and in this paper, the used Horn antennas have a 16° (from [17]) and 12° (from MIllitech) of HPBW, respectively. A_{tx} and A_{rx} are the Tx and Rx antennas, respectively. H_{tx} and H_{rx} are the Tx and Rx azimuthal HPBW, respectively.

been carried out. A spherical coordinate system of the Tx and Rx antenna is illustrated in Fig. 4. The $\Omega = (\theta,\phi)$ corresponds to the coordinate point on a spherical surface of the antenna, where $\theta \in [0,\pi]$ and $\phi \in [0,\pi]$ (for Omnidirectional $\phi \in [-\pi,\pi]$) are the elevation and azimuth angles, respectively. An illustration of the line of sight (LOS) path and the scattered paths with Horn TX antenna and omni-directional RX antenna are shown in Fig. 5. The channel parameters of l^{th} multipath is $\{L, a_l, \tau_l, \Omega_{T,l}, \Omega_{R,l}\}$, where L is the number of scattered paths, a_l is the path amplitude, τ_l is the time of arrival (TOA), $\Omega_{T,l}$ is the direction of departure (DOD) and $\Omega_{R,l}$ is the direction of arrival (DOA), respectively. The channel parameters of the LOS path is $\{a_0, \tau_0, \Omega_{T,0}, \Omega_{R,0}\}$. A modified impulse response of the scattered channel is obtained as a function of delay, DOD, and DOA as described in [18] by adding the polarizations and reflection coefficients :

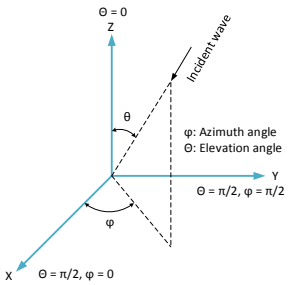

Fig. 4. The spherical coordinates of the Tx and Rx antennas.

$$h(\tau,\Omega_T,\Omega_R) = h_{los}(\tau,\Omega_T,\Omega_R) + h_s(\tau,\Omega_T,\Omega_R) \quad (1)$$

$$h_{los}(\tau,\Omega_T,\Omega_R) = a_0\,\delta(\tau-\tau_0)\delta(\Omega_T-\Omega_{T,0})\delta(\Omega_R-\Omega_{R,0}) \quad (2)$$

$$h_s(\tau,\Omega_T,\Omega_R) = \sum_{l=1}^{L} a_l\,\delta(\tau-\tau_l)\delta(\Omega_T-\Omega_{T,l})\delta(\Omega_R-\Omega_{R,l}) \quad (3)$$

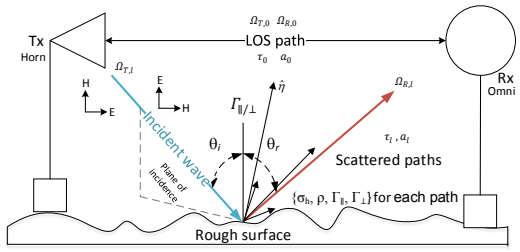

Fig. 5. An illustration of the LOS path and the scattered paths with Horn and Omnidirectional antenna configuration by considering a rough surface, where σ_h and ρ are the standard deviation of the surface heights and scattering coefficient, respectively. The θ_i and θ_r are the incident and reflected angles, respectively. The vertical or horizontal polarization direction with respect to the floor defines the electric field vector directions of the antennas towards the ceiling.

$$a_l = \{a_{l,V} \cdot \Gamma_{\parallel} \cdot \rho\}; \quad \{a_{l,H} \cdot \Gamma_{\perp} \cdot \rho\} \quad (4)$$

$$\Omega_{T,l} = \{\Omega_{T,l,V}\}; \quad \{\Omega_{T,l,H}\} \quad (5)$$

$$\Omega_{R,l} = \{\Omega_{R,l,V}\}; \quad \{\Omega_{R,l,H}\} \quad (6)$$

$$\tau_l = \{\tau_{l,V}\}; \quad \{\tau_{l,H}\} \quad (7)$$

where the equation 2 corresponds to the LOS path and the equation 3 corresponds to the scattered paths. The a_l is the l^{th} scattered path amplitude. The $a_{l,V}$ and $a_{l,H}$ are the vertical and horizontal polarized amplitudes of the l^{th} path, and $\Gamma_{\parallel}$ and $\Gamma_{\perp}$ are the corresponding reflection coefficients, respectively. The ρ is the scattering coefficient of the rough surface that can be estimated from scattering models as described in [13]. It is assumed that all scattered paths are received at the Rx within an angular range of Ω_R. The $\Omega_{T,l}$, $\Omega_{R,l}$ and τ_l which corresponds to the vertical and horizontal DOD, DOA and delay and are given in equations 5, 6 and 7, respectively. The power delay profile that characterizes the scattered channel based on antenna radiation pattern as well as polarizations, can be defined as

$$P(\tau,\Omega_T,\Omega_R) = \mathbb{E}\{|h(\tau,\Omega_T,\Omega_R)|^2\} \quad (8)$$

A. Explanations

It is assumed that the channel fading is Rician distribution since Tx and Rx are in LOS. Hence, the scattered channel can be characterized by the Rician K-factor, where K is the ratio between the power of the LOS path and the power sum of the induvidual isolated scattered paths (vertical or horizontal) $K_V = \frac{|a_{0,V}|^2}{\sum_{l=1}^{L}|a_{l,V}|^2}$ and $K_H = \frac{|a_{0,H}|^2}{\sum_{l=1}^{L}|a_{l,H}|^2}$. K_f can be used to characterize the channel as an impact factor due to the use of vertical and horizontal antenna polarizations on the scattered channel $K_f = \frac{K_V}{K_H}$. The results of time dispersion (shown in section III), K-factor, and Co-polarization ratio (CPR) (reported in [12]) demonstrate that the use of vertically polarized antennas at the Tx and Rx sides shows a probability of a higher value of RMS delay spread than the use of horizontally polarized antennas. As shown in Table II, by considering an azimuth plane, the VV configuration consists of $\pm 12^\circ$ and $\pm 360^\circ$ beamwidths whereas $\pm 12^\circ$ and $\pm 40^\circ$ of with the HH. A higher angular value from a boresight (maximum radiated power) direction provides a higher number multipath at the receiver. In addition, the rough surface may provide a higher probability of having an EM wave polarization state change, for instance by passing a wave through an anisotropic material (diffusion varies with direction). Hence, the scattered channel can be characterized by the ratio between the power with VV or HH and the power with VH or HV.

V. Conclusion

This paper presents the results of the measurements taken at 60 GHz in CANMET underground mine where different polarizations and different types of antennas are considered. Results show that a higher gallery dimension causes (which provides a higher value of TOA) a higher value of RMS delay spread. At the 40 m gallery, conspicuous 3 to 4 paths were found in contrast to the comparatively uniform low powered paths at the 70 m gallery. Results show that a higher value of antenna beamwidth provides a higher value of RMS delay spread. Due to a higher value of HPBW of the Tx and Rx antennas, the VV provides a higher value of RMS delay spread than HH one. The analysis also shows high probability of the polarization state change in this hazardous environment. The results of the time dispersion at 60 GHz suggest deploying beamforming with dual polarized directive narrow beam antennas are the most feasible to achieve high speed point to point and backhaul links inside an underground mine due to the gallery curvature and lower value of delay spread.

References

[1] S. A. M. Tariq, "Characterization and modelling of scattered wireless channel at 60 GHz in an underground mine gallery," Ph.D. dissertation, Université de Montréal-École Polytechnique, Montreal, Canada, 2016. [Online]. Available: https://publications.polymtl.ca/2289/

[2] C. Nerguizian, C. L. Despins, S. Affes, and M. Djadel, "Radio-channel characterization of an underground mine at 2.4 GHz," *IEEE Transactions on Wireless Communications*, vol. 4, no. 5, pp. 2441–2453, 2005.

[3] M. Boutin, A. Benzakour, C. L. Despins, and S. Affes, "Radio wave characterization and modeling in underground mine tunnels," *IEEE Transactions on Antennas and Propagation*, vol. 56, no. 2, pp. 540 – 549, 2008.

[4] I. Ben Mabrouk, J. Hautcoeur, L. Talbi, M. Nedil, and K. Hettak, "Feasibility of a millimeter wave MIMO system for short range wireless communications in an underground gold mine," *IEEE Transactions on Antennas and Propagation*, vol. 61, no. 8, pp. 4296–4305, Aug 2013.

[5] N. Hakem, G. Delisle, and Y. Coulibaly, "Radio-wave propagation into an underground mine environment at 2.4 GHz, 5.8 GHz and 60 GHz," in *2014 8th European Conference on Antennas and Propagation (EuCAP)*, April 2014, pp. 3592–3595.

[6] F. Yildirim, A. S. Sadri, and H. Liu, "Polarization effects for indoor wireless communications at 60 GHz," *IEEE Communications Letters*, vol. 12, no. 9, pp. 660 – 662, 2008.

[7] H. Sawada, H. Nakase, S. Kato, M. Umehira, K. Sato, and H. Harada, "Polarization dependence in double directional propagation channel at 60 GHz," in *IEEE International Symposium on Personal, Indoor and Mobile Radio Communications, PIMRC*, 2009, pp. 3010–3014.

[8] T. Manabe, K. Sato, H. Masuzawa, K. Taira, T. Ihara, Y. Kasashima, and K. Yamaki, "Polarization dependence of multipath propagation and high-speed transmission characteristics of indoor millimeter-wave channel at 60 GHz," *IEEE Transactions on Vehicular Technology*, vol. 44, no. 2, pp. 268 – 74, 1995.

[9] A. Maltsev, R. Maslennikov, A. Lomayev, A. Sevastyanov, and A. Khoryaev, "Statistical channel model for 60 GHz WLAN systems in conference room environment," *Radioengineering*, vol. 20, no. 2, pp. 409 – 22, 2011.

[10] J. Cawley, "An assessment of leaky feeder radio systems in underground mines," in *U.S. Department of the Interior Bureau of Mines*, 1989, pp. 25–1.

[11] Y.-P. Zhang, Y. Hwang, and R. Kouyoumjian, "Ray-optical prediction of radio-wave propagation characteristics in tunnel environments. 2. analysis and measurements," *IEEE Transactions on Antennas and Propagation*, vol. 46, no. 9, pp. 1337–1345, Sep 1998.

[12] S. A. M. Tariq, C. Despins, S. Affes, and C. Nerguizian, "Experimental results of Rician K-factor and co-polarization ratio of 60 GHz wireless channel in an underground mine gallery," in *2015 IEEE International Conference on Ubiquitous Wireless Broadband (ICUWB)*, Oct 2015, pp. 1–5.

[13] S. Tariq, C. Despins, S. Affes, and C. Nerguizian, "Scattering effect based on measurements of reflection coefficients at 60 GHz in an underground mine gallery," in *2014 IEEE 25th Annual International Symposium on Personal, Indoor, and Mobile Radio Communication (PIMRC)*, Sept 2014, pp. 217–221.

[14] S. A. M. Tariq, C. Despins, S. Affes, and C. Nerguizian, "Statistical modeling of 60 GHz wireless channel in an underground mine gallery," in *2015 IEEE International Conference on Ubiquitous Wireless Broadband (ICUWB)*, Oct 2015, pp. 1–5.

[15] T. Rappaport, *Wireless communications: principles and practice*, ser. Prentice Hall communications engineering and emerging technologies series. Prentice Hall PTR, 2002.

[16] B. Fleury, "First- and second-order characterization of direction dispersion and space selectivity in the radio channel," *IEEE Transactions on Information Theory*, vol. 46, no. 6, pp. 2027–2044, Sep 2000.

[17] W. L. Stutzman and G. A. Thiele, *Antenna Theory and Design*. Wiley, 2012.

[18] H. Yang, M. H. A. J. Herben, I. J. A. G. Akkermans, and P. F. M. Smulders, "Impact analysis of directional antennas and multiantenna beamformers on radio transmission," *IEEE Transactions on Vehicular Technology*, vol. 57, no. 3, pp. 1695–1707, May 2008.